Article

High-Temperature Synthesis of Ferromagnetic $Eu_3Ta_3(O,N)_9$ with a Triple Perovskite Structure

Jhonatan R. Guarín, Carlos Frontera, Judith Oró-Solé, Jaume Gàzquez, Clemens Ritter, Josep Fontcuberta,* and Amparo Fuertes*

Read Online

ACCESS | Metrics & More | Article Recommendations

ABSTRACT: Europium tantalum perovskite oxynitrides were prepared by a new high-temperature solid-state synthesis under N_2 or N_2/ H_2 gas. The nitrogen stoichiometry was tuned from 0.63 to 1.78 atoms per Eu or Ta atom, starting with appropriate N/O ratios in the mixture of the reactants Eu_2O_3, EuN and Ta_3N_5, or Eu_2O_3 and TaON, which was treated at 1200 °C for 3 h. Two phases were isolated with compositions $EuTaO_{2.37}N_{0.63}$ and $Eu_3Ta_3O_{3.66}N_{5.34}$, showing different crystal structures and magnetic properties. Electron diffraction and Rietveld refinement of synchrotron radiation X-ray diffraction indicated that $EuTaO_{2.37}N_{0.63}$ is a simple perovskite with cubic $Pm\bar{3}m$ structure and cell parameter $a = 4.02043(1)$ Å, whereas the new compound $Eu_3Ta_3O_{3.66}N_{5.34}$ is the first example of a triple perovskite oxynitride and shows space group $P4/mmm$ with crystal parameters $a = 3.99610(2)$, $c = 11.96238(9)$ Å. The tripling of the c-axis in this phase is a consequence of the partial ordering of europium atoms with different charges in two A sites of the perovskite structure with relative ratio 2:1, where the formal oxidation states +3 and +2 are respectively dominant. Magnetic data provide evidence of ferromagnetic ordering developing at low temperatures in both oxynitrides, with saturation magnetization of about 6 μ_B and 3 μ_B per Eu ion for $EuTaO_{2.37}N_{0.63}$ and the triple perovskite $Eu_3Ta_3O_{3.66}N_{5.34}$ respectively, and corresponding Curie temperatures of about 7 and 3 K, which is in agreement with the lower proportion of Eu^{2+} in the latter compound.
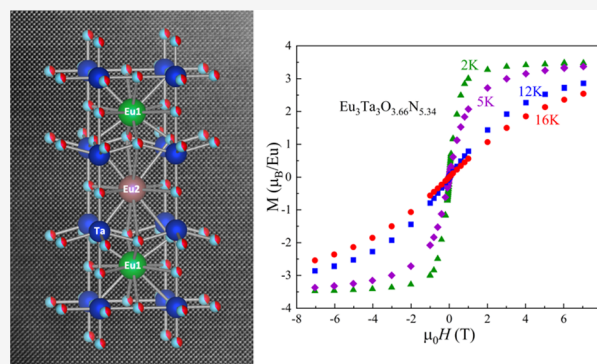
INTRODUCTION

Perovskite oxynitrides $AB(O,N)_3$ (A = alkaline earth or rare earth metal; B = transition) are important materials with electronic properties and photocatalytic activity of relevance in several reactions.[1] The majority of reported compounds show crystal structures derived from the $Pm\bar{3}m$ aristotype, frequently showing lower symmetry space groups resulting from a combination of octahedral tilting and anion order.[2–4] Perovskite oxynitrides with more complex structures have been also reported, although the number of compounds is restricted to a few examples. Double perovskites with B-site order $A_2B'B''(O,N)_6$ have been reported for three compounds with the pairs of cations $B'/B'' = Fe^{3+}/W^{6+}$,[5] Fe^{3+}/Mo^{6+},[6] and Mn^{2+}/Ta^{5+}.[7] Layered Ruddlesden–Popper[8,9] ($A_{n+1}B_nO_{3n+1}$) phases with $n = 1$ ($A_2B(O,N)_4$) and $n = 2$ ($A_3B_2(O,N)_7$) have been reported for six compounds containing Nb,[10] Ta,[11–13] or Al,[14] and Dion-Jacobson structures[15,16] $A'[A''_{n-1}B_n(O,N)_{3n+1}]$ have been found for A' = alkaline metal, A'' = La, Ca, and B = Ta, Nb.[17,18] In the group of hexagonal perovskite oxynitrides, the only known compound is $BaWON_2$ that shows the 6H polytype.[19]

Europium perovskite oxynitrides $EuB(O,N)_3$ (B = Ti, Nb, W, Ta) have been investigated for their electrical and magnetic properties, which are affected by the N/O balance that tunes the formal valence state of Eu and the B cations: Eu^{2+} to Eu^{3+}, and those of transition metals Nb^{4+}, Nb^{5+}, W^{5+}, and W^{6+}. For instance, $EuNbO_{2+x}N_{1-x}$ ($x \leq 0.14$)[20] and $EuWO_{1+x}N_{2-x}$ ($-0.16 \leq x \leq 0.46$)[21] show ferromagnetic ordering of Eu^{2+} $S = 7/2$ spins below 5.2 and 12 K, respectively. In $EuWO_{1+x}N_{2-x}$, the electrical conductivity changes with the N/O ratio, and in both Nb and W compounds colossal magnetoresistance emerges below the Curie temperature, arising from the coupling between the localized Eu^{2+} spins and the transition metal (4,5)d carriers. $EuTiO_{3-x-y}N_x$ with nitrogen contents up to $x = 1$ has been also reported,[22] with
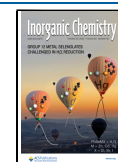
the N/O ratio and the anion vacancies tuning the europium oxidation state and the electronic properties.

The europium tantalum oxynitride perovskite $EuTaO_2N$ was first prepared by Marchand et al. by the treatment of $EuTaO_4$ under NH_3 at 950 °C.[23] More recently, we prepared this oxynitride in similar conditions with a small nitrogen nonstoichiometry $EuTaO_{2-x}N_{1+x}$ ($0 \leq x \leq 0.2$), formally involving the presence of a low proportion of Eu^{3+} for $x > 0$, and ferromagnetism was observed below $T_c = 5.1$ K for a sample with $x = 0.05$. The laboratory X-ray diffraction pattern of the $EuTaO_2N$ sample could be indexed in a cubic cell with $a = 4.0217(2)$ Å, but synchrotron X-ray diffraction indicated a small tetragonal distortion with $a = 4.02054(2)$, $c = 4.03079(4)$ Å.[20] Electron diffraction of $EuTaO_2N$, $EuNbO_2N$, and $EuWO_2N$ shows a $\sqrt{2}a_0 \times \sqrt{2}a_0 \times 2a_0$ superstructure (where a_0 is the parameter of the perovskite cubic subcell) that was ascribed to octahedral tilting.[20,21] Disordered B-site perovskites with compositions $EuTi_{0.5}W_{0.5}O_{3-x}N_x$ and nitrogen contents between 0.87 and 1.63 show ferromagnetic and antiferromagnetic exchange interactions between the Eu^{2+} cations, and the magnetic properties are tuned by the equilibrium $Eu^{2+} + W^{6+} \leftrightarrow Eu^{3+} + W^{5+}$ which is shifted to the right for larger x values.[24]

The synthesis of all previously reported europium perovskite oxynitrides has been performed by ammonolysis of precursors at temperatures below 1000 °C. In this paper, we report the study of the crystal structure and magnetic properties of $EuTaO_{3-x}N_x$ compounds with a large range of N/O contents, prepared by a new synthetic approach that uses solid-state reactions between metal nitrides and oxides under N_2 or N_2/H_2 gas at relatively high temperature (1200 °C). Two phases have been isolated with $EuTaO_{2.37}N_{0.63}$ and $Eu_3Ta_3O_{3.66}N_{5.34}$ stoichiometries showing different perovskite structures, as determined from synchrotron X-ray diffraction and electron diffraction. $EuTaO_{2.37}N_{0.63}$ is a simple Eu^{2+} cubic perovskite similar to previously reported $EuTaO_2N$ but with a large proportion (37%) of reduced Ta^{4+}. The compound $Eu_3Ta_3O_{3.66}N_{5.34}$ represents the first example of an oxynitride with a triple perovskite structure, which is a consequence of the partial ordering of Eu^{2+} and Eu^{3+} ions in the A sites. The magnetic data are found to be fully consistent with this finding, with both oxynitrides displaying a ferromagnetic ordering at low temperatures, with Curie temperatures of about 7 K for $EuTaO_{2.37}N_{0.63}$ and somewhat lower (≈ 3 K) for $Eu_3Ta_3O_{3.66}N_{5.34}$ due to dilution effects of magnetic interactions in the latter compound.

EXPERIMENTAL METHODS

Synthesis and Chemical Characterization. Samples of 130 mg with compositions $EuTaO_{3-x}N_x$ ($0.63 \leq x \leq 1.78$) were prepared using the reactants Eu_2O_3 (Sigma-Aldrich 99.9%), EuN (Materion, 99.9%), TaON, and Ta_3N_5. The N/O ratio in the initial mixture was the most determining factor in the final nitrogen content of the sample. This was changed by varying the proportion of the reactants while keeping constant the Eu/Ta ratio of 1:1. Eu_2O_3 was treated at 900 °C under a dynamic vacuum of 10^{-3} Torr for dehydration. Ta_3N_5 was prepared by the treatment of Ta_2O_5 (Sigma-Aldrich 99.99%) at 850 °C under $NH_3(g)$ (Carburos Metálicos, 99.9%), at a flow rate of 600 cm^3/min, using several cycles of 15 h with intermediate regrinding. TaON was prepared by the treatment of Ta_2O_5 at the same temperature under $NH_3(g)$ at a flow rate of 40 cm^3/min, using two cycles of 3 h with intermediate regrinding.[25] Handling of the reactants, mixing, and pelletizing were done in a glovebox under a recirculating Ar atmosphere. The pellets were placed in a

molybdenum crucible covered by zirconium foil, which was also used for oxygen and water scavenging in a second crucible placed close to the sample in the furnace tube (Al_2O_3, Alsint 99.7%). The samples were heated at 300 °C/h up to 1200 °C under flowing N_2 (Air Liquide, 99.9999%) or N_2/H_2 (95%/5% v/v, Air Liquide, 99.9999%), treated for 3 h at 1200 °C, and cooled down to room temperature.

Nitrogen contents were determined by combustion analysis performed in a ThermoFisher Scientific instrument, heating the samples in oxygen up to 1060 °C and using MgO, WO_3, and Sn as additives and atropine as a reference standard. EDX analyses of cation contents were performed in a FEI Quanta 200 FEG microscope equipped with an EDAX detector with an energy resolution of 132 eV. The analyses were performed on 10−15 crystallites for each sample.

Structural Characterization. Laboratory X-ray powder diffraction data were acquired on a Panalytical X'Pert Pro MPD diffractometer using Cu Kα radiation ($\lambda = 1.5418$ Å). High-resolution synchrotron X-ray powder diffraction data were measured at room temperature from capillary samples (0.3 mm diameter) in the angular range $2.0° \leq 2\theta \leq 56.9°$ at the MSPD beamline[26] of the ALBA Synchrotron (Cerdanyola del Vallès, Spain). A short wavelength of 0.45872 Å calibrated with Si NIST was selected by using a double Si(111) and Si(220) crystal monochromator. Background refinement was performed by linear interpolation, and data were corrected from absorption.
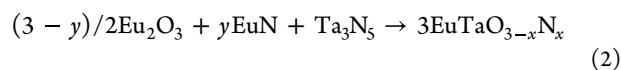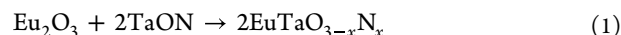
Neutron powder diffraction data were collected for 12 h at room temperature on the high-intensity D20 diffractometer at the Institut Laue-Langevin (ILL), France. In order to reduce the absorption from Eu, a double wall vanadium can was used as a sample holder, and a short wavelength of 1.37 Å at the high 118° take-off angle giving high resolution was chosen. The step scanning mode where the detector was moved in 61 steps of 0.05° was chosen in order to compensate for the nonperfect calibration of the more than 3000 detector cells. Rietveld analysis was carried out using the program Fullprof.[27]

Electron diffraction micrographs were obtained in a JEOL 1210 transmission electron microscope operating at 120 kV using a side entry double tilt $\pm 60°/\pm 30°$ specimen holder. The samples were prepared by dispersing the powders in hexane and depositing a droplet of the suspension on a copper grid coated with a holey carbon film. The local microstructure of the samples was analyzed by means of scanning transmission electron microscopy (STEM) on a ThermoFisher Spectra 300 operated at 300 kV. The high-angle annular dark field detector allows for recording incoherent Z-contrast images, in which the contrast of an atomic column is approximately proportional to the square of the average atomic number (Z). Accordingly, it is possible to distinguish between Ta and Eu. The experiments were performed in the Joint Electron Microscopy Center at ALBA (Cerdanyola del Vallès, Spain).

Magnetic Measurements. Magnetic measurements were performed at fields of 25 Oe and 10 kOe between 2 and 300 K using a Quantum Design SQUID magnetometer. Magnetization-field loops were measured between −70 and +70 kOe between 2 and 16 K.

RESULTS AND DISCUSSION

Synthesis and Structural Study of $EuTaO_{2.37}N_{0.63}$ and $Eu_3Ta_3O_{3.66}N_{5.34}$. The synthesis of europium tantalum perovskite oxynitride samples is performed at high temperatures under N_2/H_2 (95%/5% v/v) or N_2 gas, using one of the following solid-state reactions with one single treatment of 3 h at 1200 °C

$$Eu_2O_3 + 2TaON \rightarrow 2EuTaO_{3-x}N_x \qquad (1)$$

$$(3-y)/2Eu_2O_3 + yEuN + Ta_3N_5 \rightarrow 3EuTaO_{3-x}N_x \qquad (2)$$

The reaction used, the proportions of the reactants, the selected gas, and the maximum synthesis temperature

determined the average nitrogen content of the sample per Eu or Ta mol, which was tuned from $x = 0.63$ to 1.78, and the phase composition. We have recently reported a similar synthetic approach for the preparation of $LaTaON_2$ and slightly nitrogen-deficient $LaTaO_{1.12}N_{1.88}$ that we investigated for their dielectric properties.[28] Both compounds were prepared either from LaN and TaON or from La_2O_3, LaN, and Ta_3N_5 at 1500 °C. In the $EuTaO_{3-x}N_x$ samples, the syntheses performed at 1500 °C led to partial decomposition into TaN and Eu_3TaO_6 phases; hence, a lower temperature of 1200 °C was selected.

Two different perovskite phases were isolated, with stoichiometries $EuTaO_{2.37}N_{0.63}$ (phase I) and $Eu_3Ta_3O_{3.66}N_{5.34}$ (phase II) that showed black and brown colors, respectively. The Eu/Ta ratios using EDX analysis were 0.93(6) for phase I and 0.94(10) for phase II, whereas the errors in the nitrogen contents obtained by combustion analysis were ±0.03 in both cases. The oxygen stoichiometry was calculated by difference, assuming that the total anion content was, respectively, three and six atoms per formula for phases I and II. $EuTaO_{2.37}N_{0.63}$ was prepared using reaction 1 in N_2/H_2 (95%/5% v/v) gas, which favored the reduction of the cations. The observed nitrogen content in this sample involved a decrease in the N/O ratio with respect to the initial composition (from 0.4 to 0.27). Considering the charge compensation, this stoichiometry is consistent with the presence of reduced Ta and Eu cations with the formal plausible composition $Eu^{2+}(Ta_{0.37}{}^{4+}Ta_{0.63}{}^{5+})$-$O_{2.37}N_{0.63}$. The existence of 100% of europium in the divalent state agrees with the observed effective magnetic moment of this compound (see below), whereas the +4 oxidation state of tantalum has been suggested in other perovskite oxynitrides coexisting with the more stable Ta^{5+} cation.[28−30] The electron diffraction patterns of $EuTaO_{2.37}N_{0.63}$ indicated a cubic perovskite cell of $a \simeq 4.0$ Å with the space group of aristotype $Pm\bar{3}m$ (Figure 1). This result differs from our previously
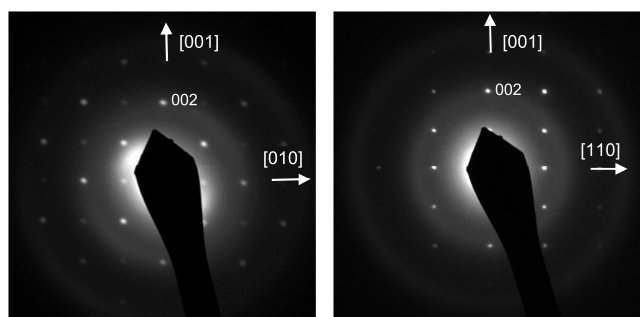

Figure 1. Electron diffraction patterns along the [100] and [$\bar{1}$10] axes of $EuTaO_{2.37}N_{0.63}$.

reported electron diffraction study of $EuTaO_2N$ prepared by ammonolysis, which showed additional reflections indicative of a tilted $I2/m$ superstructure with $a, b = \sqrt{2} a_0$ and $c = 2 a_0$.[2,20] The perovskite $Eu_3Ta_3O_{3.66}N_{5.34}$ (phase II) was prepared with reaction 2 at the same temperature than $EuTaO_{2.37}N_{0.63}$, under N_2 with $y = 1.8$ (initial ratio N/O of 3.78). The electron diffraction patterns of this phase showed a $3 \times a_0$ super-structure along one of the axes of the perovskite subcell (Figure 2). The reconstruction of the reciprocal lattice leads to a tetragonal cell with parameters $a \simeq 4.04$, $c \simeq 12.08$ Å and reflection conditions compatible with the space group $P4/mmm$. The study by electron diffraction of samples prepared
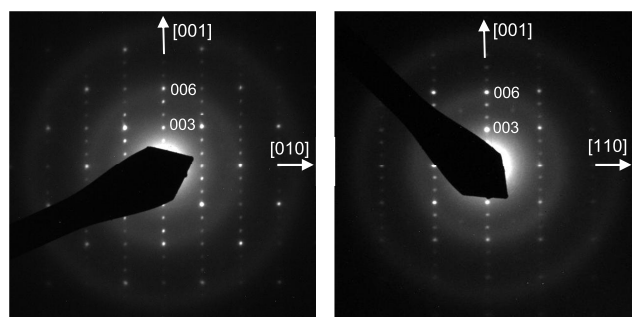

Figure 2. Electron diffraction patterns along the [100] and [$\bar{1}$10] axes of $Eu_3Ta_3O_{3.66}N_{5.34}$.

using reaction 2 but starting with N/O ratios below 3.78 invariably led to the observation of a coexistence of two phases: the compound II and an additional perovskite phase, with symmetry $I2/m$ and $a, b = \sqrt{2}a_0$ and $c = 2a_0$, which is the same as previously reported for our $EuTaO_2N$ sample prepared by ammonolysis.[20] The biphasic nature of these samples was also clearly observed in the laboratory X-ray diffraction patterns.

Rietveld refinement of synchrotron X-ray diffraction data of $EuTaO_{2.37}N_{0.63}$ (Figure 3) was performed in the space group $Pm\bar{3}m$ with $a = 4.02044(1)$ Å ($V = 64.986$ Å^3), using a common temperature factor for all atoms $B = 0.818(2)$ Å^2. The observed bond distances are $d(Eu−O,N) = 2.843$ Å and $d(Ta−O,N) = 2.010$ Å. The cell parameter is close to that shown by $EuTaO_2N$ ($a = 4.0217(2)$ Å) prepared by ammonolysis,[20] indicating that the decrease in a caused by the lower nitrogen content ($r(N^{3−}) = 1.46$ Å vs $r(O^{2−}) = 1.38$ Å both for CN = IV) is compensated by the increase induced by the presence of Ta^{4+} ($r(Ta^{5+}) = 0.64$ Å, $r(Ta^{4+}) = 0.68$ Å, both for CN = VI).[31]

The synchrotron X-ray powder diffraction of $Eu_3Ta_3O_{3.66}N_{5.34}$ (Figure 4) did not show clearly visible superstructure peaks of the triple cell, but a tetragonal splitting is observed for several reflections even at low angles, as well as significant broadening in all peaks with respect to the cubic compound $EuTaO_{2.37}N_{0.63}$ (see Figure 5). A Rietveld refine-ment in a tetragonal subcell with parameters $a = 3.98994(2)$, $c = 3.9968(5)$ Å and space group $P4/mmm$ was performed with one position for Eu and Ta at sites 1d and 1a respectively, and two anion positions at 0, 1/2, 0 (2f site) and 0, 0, 1/2 (1b site). This led to poor agreement factors, with $R_{Bragg} = 8.45\%$, $R_{wp} = 7.97\%$, and $\chi^2 = 4.90$. In contrast, the refinement performed using a triple perovskite structure model with parameters $a = 3.99610(2)$, $c = 11.96238(9)$ Å in the space group $P4/mmm$ and two crystallographically independent sites for both Eu and Ta atoms (Figures 4 and 6 and Table 1) showed significantly improved agreement factors, with $R_{Bragg} = 5.64\%$, $R_{wp} = 7.19\%$, and $\chi^2 = 3.74$. For the nitrogen and oxygen atoms, we considered a statistical distribution in the four available sites, because the X-rays do not provide enough contrast between the two anions. In order to investigate the potential anion order, neutron diffraction data were acquired on a 380 mg sample prepared in the same conditions as $Eu_3Ta_3O_{3.66}N_{5.34}$, that showed close nitrogen content (1.91(3) atoms per perovskite unit), similar electron diffraction patterns, and refined parameters from X-ray diffraction $a = 3.98919(2)$, $c = 12.00107(11)$ Å. These data clearly showed superstructure peaks that were indexed in the triple perovskite unit cell. However, the large absorption cross-section of europium and
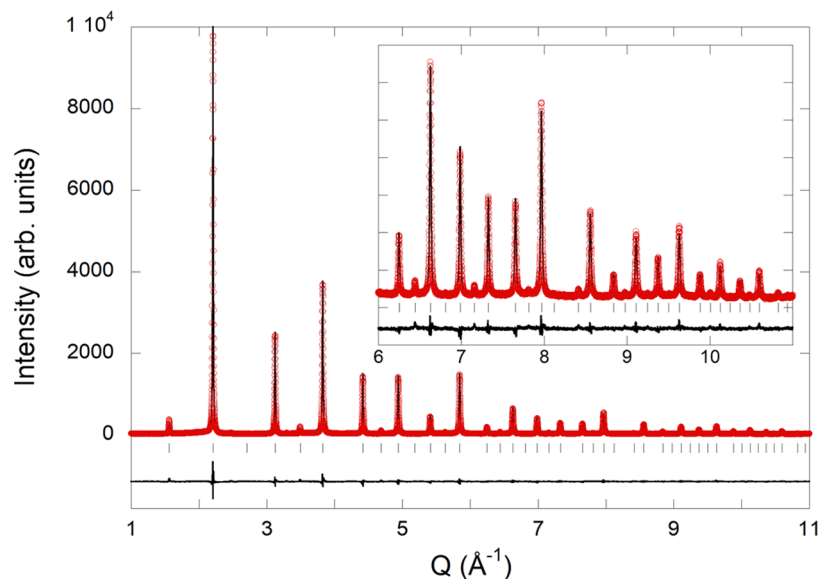
Figure 3. Rietveld fit to synchrotron X-ray powder diffraction pattern of $EuTaO_{2.37}N_{0.63}$ performed in space group $Pm\bar{3}m$ with a = 4.02044(1) Å. The inset shows the high Q region enlarged (where $Q = (4\pi \sin\theta)/\lambda$). Agreement factors: R_{Bragg} = 3.73%, R_p = 4.76%, R_{wp} = 6.13%, χ^2 = 4.03.

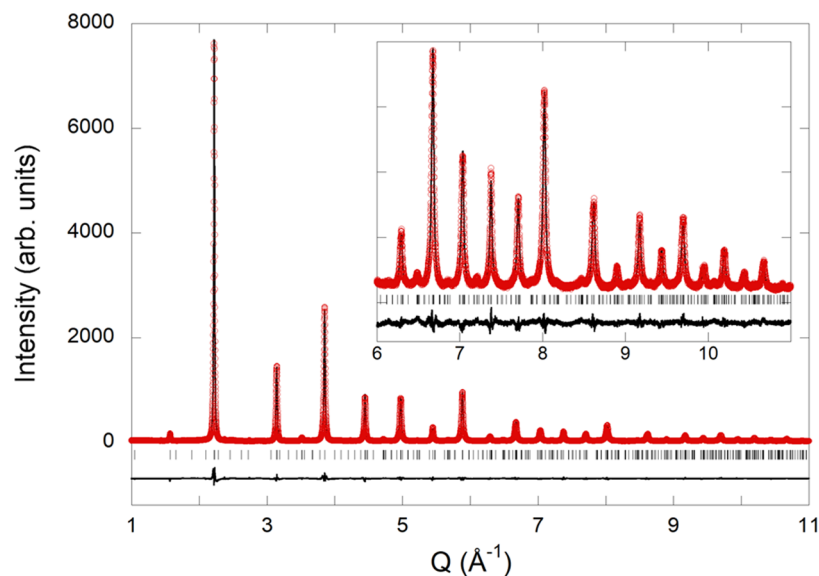**Figure 4.** Rietveld fit to synchrotron X-ray powder diffraction pattern of $Eu_3Ta_3O_{3.66}N_{5.34}$ performed in the $P4/mmm$ space group with parameters a = 3.99610(2), c = 11.96238(9) Å. The inset shows the high Q region enlarged.

the small sample mass strongly limited the quality of the data and prevented the extraction of reliable structural data from the Rietveld refinement. A Le Bail fit performed using the Fullprof program without introducing any structural model returned the refined parameters a = 4.0262(2) and c = 12.0959(7) Å (Figure 7). The small deviations between the cell parameters obtained by neutron diffraction and X-ray diffraction for this sample are due to differences in the resolution and quality between the two sets of data, caused by the strong Eu absorption in neutron diffraction.

The structural data in Table 1 show that the observed average bond distance around the europium atom at the 1d site (d(Eu2−O,N) = 3.090 Å) is significantly larger than for Eu1 at the 2h site (2.711 Å). Considering charge compensation and the analyzed nitrogen stoichiometry of this sample (1.78 per Eu mol), phase II is formally mixed-valence $Eu_{2.34}{}^{3+}Eu_{0.66}{}^{2+}Ta_3O_{3.66}N_{5.34}$. According to the structural data

and the differences in the ionic radii between Eu^{2+} and Eu^{3+} (r Eu^{3+}(CN IX) = 1.120 Å vs r Eu^{2+}(CN IX) = 1.30 Å),[31] the triple perovskite structure is plausibly formed from two ordered A sites A1 and A2 with different charge and ratio 2:1, that show preferred occupancy by Eu^{3+} and Eu^{2+} respectively creating distinct anion environments. A recent example of mixed-valence europium tantalum oxynitride is the n = 2 Ruddlesden−Popper compound $Eu^{2+}Eu_2{}^{3+}Ta_2O_3N_4$ that shows, as $Eu_{2.34}{}^{3+}Eu_{0.66}{}^{2+}Ta_3O_{3.66}N_{5.34}$, a larger proportion of Eu^{3+} related to Eu^{2+}. In $Eu^{2+}Eu_2{}^{3+}Ta_2O_3N_4$, the Eu^{2+} and Eu^{3+} cations order respectively in the rock-salt and in the perovskite-type positions of the Ruddlesden−Popper structure.[13] The unit-cell volumes of the two europium tantalum perovskites $EuTaO_{2.37}N_{0.63}$ and $Eu_3Ta_3O_{3.66}N_{5.34}$ are V_I = 64.986 Å³ and V_{II} = 191.025(2) Å³ respectively, which after normalizing to the cubic perovskite subcell (64.986 and 63.675 Å³ respectively) show a decrease with increasing the nitriding
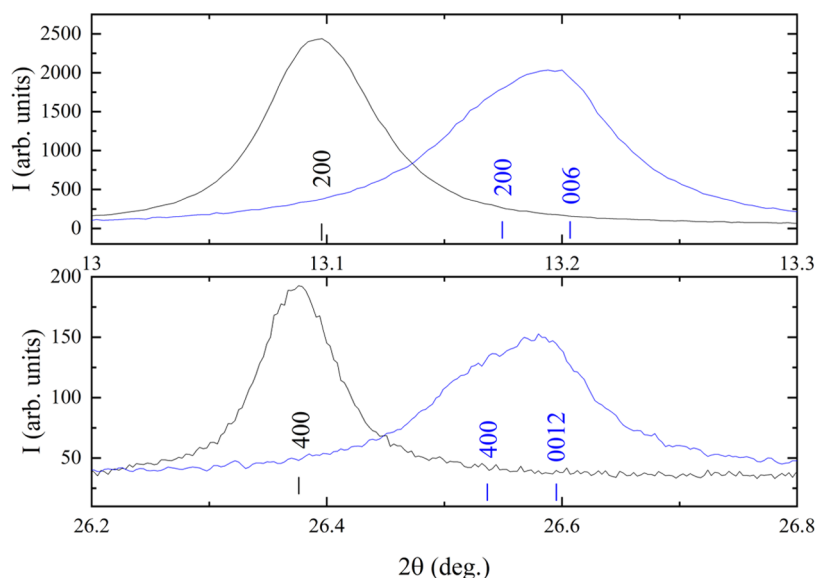
Figure 5. Synchrotron X-ray powder diffraction profiles in two 2θ regions of $EuTaO_{2.37}N_{0.63}$ and $Eu_3Ta_3O_{3.66}N_{5.34}$ are depicted in black and blue colors, respectively.

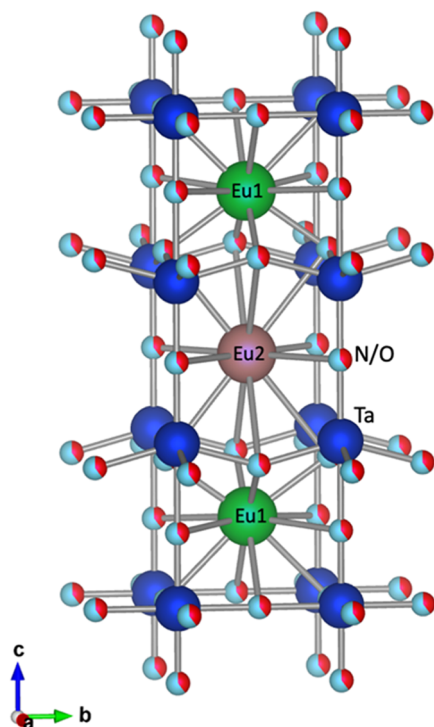**Figure 6.** Structural model of the triple perovskite $Eu_3Ta_3O_{3.66}N_{5.34}$.

degree. This is a consequence of the oxidation of the cations that overcompensates the increase caused by the larger radius of N^{3-} compared to O^{2-}.

Figure 8a shows a high-resolution Z-contrast image of a $Eu_3Ta_3O_{3.66}N_{5.34}$ grain viewed along the [100] zone axis. The Fourier Transform (FT) of the image clearly shows the superstructure peaks of the triple cell (indicated by a red bracket). Figure 8b displays a higher-resolution Z-contrast image with a magnified view of the superstructure. Notice that every three planes of Ta one is more intense, which allows us to identify and pinpoint the triple perovskite (see yellow arrows in Figure 8b and the intensity profile along the c-axis

shown in Figure 8c). This is due to the fact that this compound contains two types of Ta−O/N planes (see Figure 6), one with the anions perfectly aligned with Ta cations (Ta2 positions) and another with the anions slightly above or below the Ta plane (Ta1 sites), ensuing slightly dimmer Ta atomic columns compared with the former ones.

Magnetic Properties. In Figure 9a−d, we summarize the magnetic properties of $EuTaO_{2.37}N_{0.63}$ (phase I) and $Eu_3Ta_3O_{3.66}N_{5.34}$ (phase II). As previously stated, according to the stoichiometric ratios, the charge balance is expected to be (I) $Eu^{2+}Ta_{0.63}{}^{5+}Ta_{0.37}{}^{4+}O_{2.37}N_{0.63}$ and (II) $Eu_{2.34}{}^{3+}Eu_{0.66}{}^{2+}Ta_3{}^{5+}O_{3.66}N_{5.34}$.

The temperature-dependent magnetic susceptibility $\chi(T)$ of phase I is expected to display Curie−Weiss (CW) behavior governed by the presence of Eu^{2+} ($4f^7$ (^8S)) ions having localized $S = 7/2$ spin. The presence of $5d^1$ electrons (Ta^{4+} ions) in a partially occupied broadband is expected to produce a marginal temperature-independent Pauli paramagnetism that will add to any diamagnetic contribution. Accordingly, $\chi(T)$ is given by

$$\text{phase I: } \chi(T) = \frac{C(Eu^{2+})}{(T - \theta_{CW})} + \chi_0 \tag{3}$$

where $C(Eu^{2+})$ is the corresponding Curie constant and θ_{CW} is the extrapolated Curie temperature that give a measure of the strength of the magnetic interactions between the spins, eventually ordered at low temperature. χ_0 contains temperature-independent paramagnetic and diamagnetic susceptibilities. If the $5d^1$ electrons are spin-polarized by the magnetic moments of Eu^{2+} ions, a departure from the $\chi(T)$ dependence described by eq 3 is expected. This has been observed for instance in Sr_2FeMoO_6,[32] where localized moments of 3d-$Fe^{2+/3+}$ ions induce a spin polarization in the conduction band (4d-Mo^{4+}).

For $Eu_3Ta_3O_{3.66}N_{5.34}$ (phase II), the presence of localized moments at Eu^{2+} ions should produce a CW contribution to $\chi(T)$ as described above, of relative weight "$n_{Eu^{2+}}$" combined with the temperature-dependent van Vleck contribution of the magnetic moment of Eu^{3+}.[33,34] Notice that although Eu^{3+} in its

Table 1. Summary of the $P4/mmm$ Model for $Eu_3Ta_3O_{3.66}N_{5.34}$ Refined against Room Temperature Synchrotron X-ray Powder Diffraction Data Using λ= 0.45872 Å[a,b,c]

atom	site	x	y	z	occupancy
Eu1	2h	0.5	0.5	0.1690(2)	1
Eu2	1d	0.5	0.5	0.5	1
Ta1	2g	0	0	0.33464(15)	1
Ta2	1a	0	0	0	1
O1/N1	2g	0	0	0.1522(13)	0.4/0.6
O2/N2	4i	0.5	0	0.2887(6)	0.4/0.6
O3/N3	1b	0	0	0.5	0.4/0.6
O4/N4	2f	0.5	0	0	0.4/0.6

bond	distance (Å)	bond	distance (Å)	bond	distance (Å)
Eu1−O1,N1	2.833(1) × 4	Eu1−O2,N2	2.458(4) × 4	Eu1-(O4,N4)	2.842(2) × 4
Eu2−O2,N2	3.222(6) × 8	Eu2−O3,N3	2.826 × 4		
Ta1−O1,N1	2.182(16) × 2	Ta1−O2,N2	2.072(2) × 2	Ta1−O3,N3	1.978(2) × 2
Ta2−O1,N1	1.821(16) × 2	Ta2−O4,N4	1.998 × 4		

[a]Cell parameters: a = 3.99610(2), c = 11.96238(9) Å. V = 191.025(2) Å^3. R_{Bragg} = 5.64%, R_{wp} = 7.19%, χ^2 = 3.74. [b]Average bond distances (Å): Eu1−O,N 2.711; Eu2−O,N 3.090; Eu−O,N 2.90; Ta1−O,N 2.078; Ta2−O,N 1.939. Bond angles (deg): Ta1-(O2,N2)-Ta1 149.2(3). [c]Estimated standard deviations in parentheses are shown once for each independent variable. Isotropic thermal parameters were refined to B = 0.657(3) Å^2 for all sites.
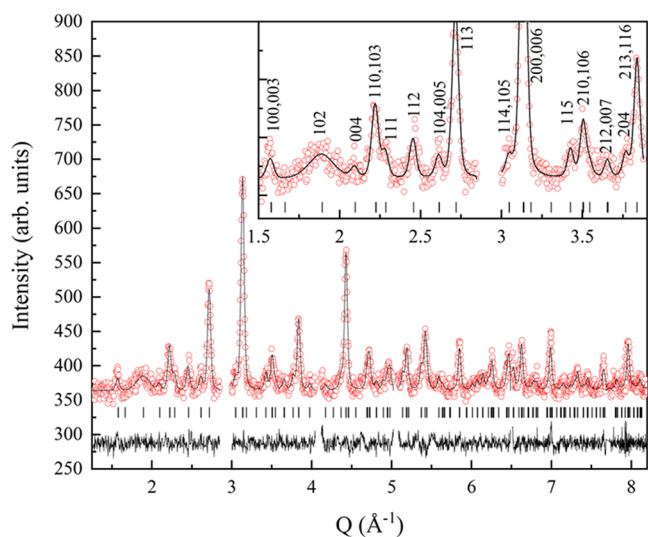

Figure 7. Le Bail fit of neutron diffraction data for phase II (λ = 1.37 Å) indexed (inset) in a $P4/mmm$ unit cell with parameters a = 4.0265(2) and c = 12.0949(12) Å. Excluded regions correspond to peaks from the V sample holder.

Figure 8. (a) High-resolution Z-contrast image of the $Eu_3Ta_3O_{3.66}N_{5.34}$ triple perovskite compound viewed along the [100] zone axis. The inset shows the Fourier Transform of the Z-contrast image, in which the extra Bragg stemming from the superstructure is indicated with a red bracket. (b) Atomic-resolution Z-contrast image of $Eu_3Ta_3O_{3.66}N_{5.34}$ phase viewed along the [100] zone axis. Yellow arrows point to the more intense Ta−O/N planes. The inset shows a sketch of the $Eu_3Ta_3O_{3.66}N_{5.34}$ triple perovskite structure along the [100] zone axis. (c) Two unit-cell-averaged intensity profiles along the direction of the orange arrow are shown in (b). Ta, Eu, O, and N atoms are represented with blue, green/pink, red, and blue circles, respectively.

ground state is nonmagnetic ($^7F_0$), thermal excitation to higher lying states (for instance the first one ($^7F_1$) is only at about 46 meV[33] and shall produce a temperature-dependent magnetic susceptibility that will add to the Eu^{2+} contribution, of weight $(1 - n_{Eu^{2+}})$, and to any diamagnetic contribution). Accordingly, the magnetic susceptibility per Eu ion can be expressed as

$$\text{phase II: } \chi(T) = n_{Eu^{2+}}\frac{C(Eu^{2+})}{(T - \theta_{CW})} + (1 - n_{Eu^{2+}})\chi_{Eu^{3+}}(T)$$
$$+ \chi_0 \qquad (4)$$

The magnetic susceptibility recorded at 10 kOe of these compounds displays roughly high-temperature CW behavior (Figure 9a, right axis), where some curvature can be readily appreciated more apparently for phase II than for phase I, as expected from eqs 3 and 4.
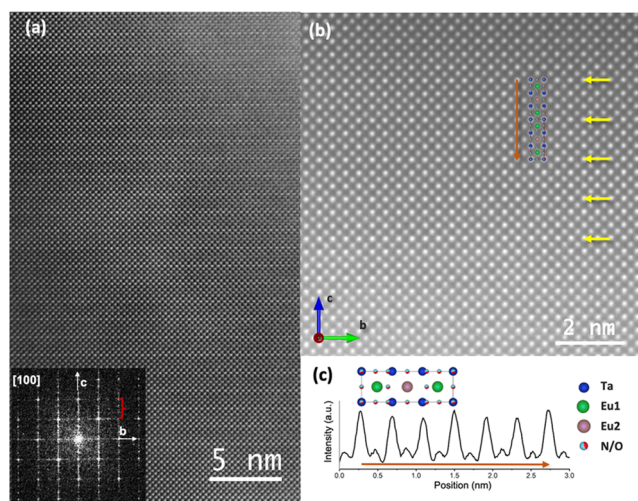
Equation 3 and 4 have been used to fit the data for $EuTaO_{2.37}N_{0.63}$ and $Eu_3Ta_3O_{3.66}N_{5.34}$, respectively. The van Vleck contribution to the susceptibility of Eu^{3+} was computed using an excitation energy of 46 meV as given in ref 33. Continuous lines through the data in Figure 9a are the results of fitting eqs 3 and 4 to the experimental $\chi(T)$ curves and the corresponding fitted parameters are listed in Table 2.

Data in Table 2 reflect the dominating presence of Eu^{2+} ions in $EuTaO_{2.37}N_{0.63}$. The extracted effective moment ($\mu_{eff} \approx 7.44$ μ_B/f.u.) compares well with the expected one (7.94 μ_B/f.u.) for Eu^{2+} ($S = 7/2$) ions. The extracted θ_{CW} ($\approx$4.7 K) implies that
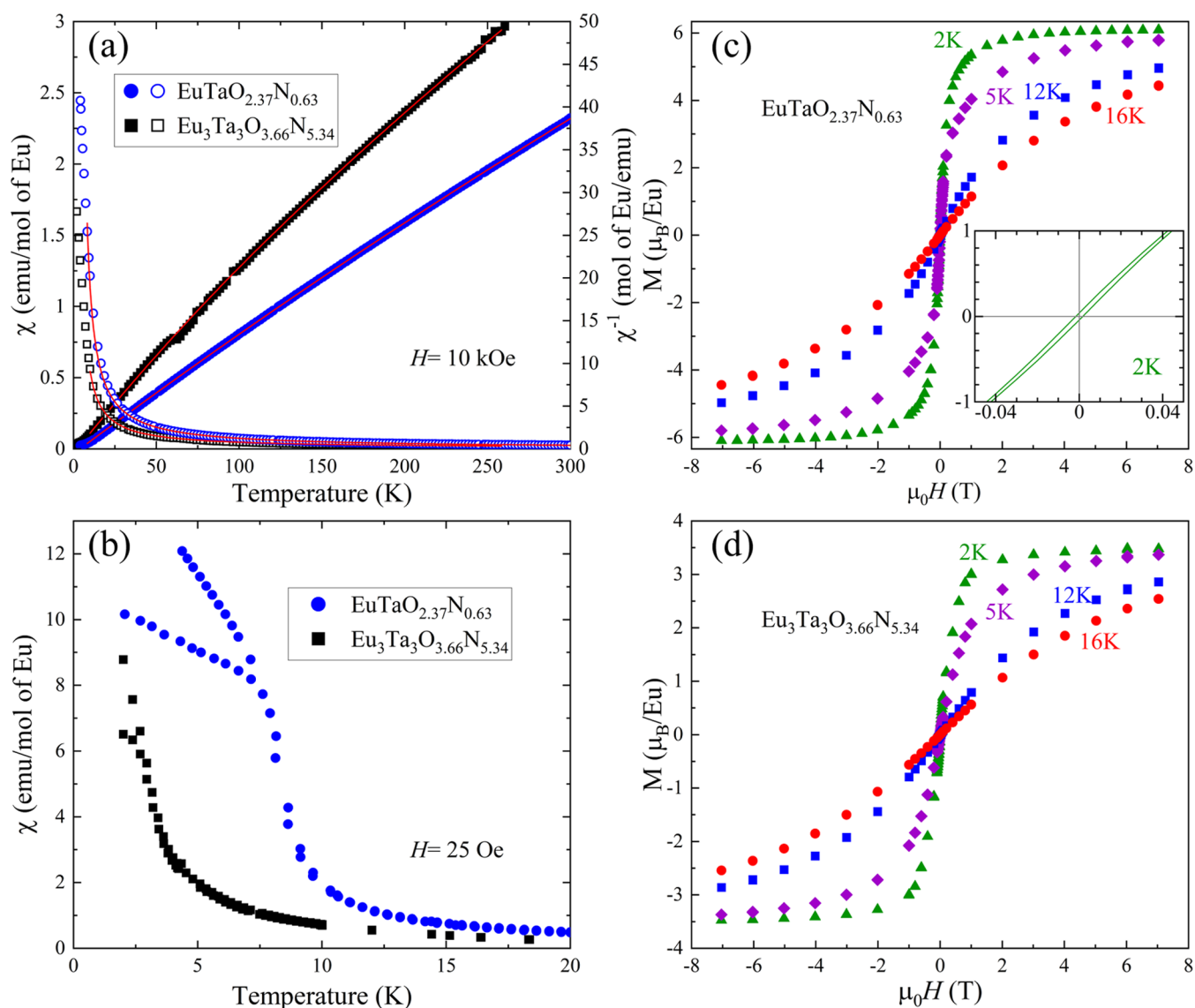
Figure 9. (a) Temperature dependence of the magnetic susceptibility recorded at 10 kOe (left axis) and the inverse susceptibility (right axis) of EuTaO$_{2.37}$N$_{0.63}$ and Eu$_3$Ta$_3$O$_{3.66}$N$_{5.34}$ together with the fitted values according to eqs 3 and 4, respectively. (b) Temperature dependence of the magnetic susceptibility recorded at a low magnetic field (25 Oe) after zero-field and field-cooling (ZFC-FC) for the same compounds. The corresponding magnetization loops collected between 2 and 16 K are shown in (c,d). Inset in (c) is a zoom of the magnetization loop at 2 K in the low field (<400 Oe) region.

Table 2. Parameters Obtained from Fittings to Magnetic Susceptibility Data of EuTaO$_{2.37}$N$_{0.63}$ Using Equation 3, and for Eu$_3$Ta$_3$O$_{3.66}$N$_{5.34}$ Using Equation 4 by Fixing

$$\mu_{\text{eff}}^{\text{Eu}^{2+}} = 2\sqrt{\frac{7}{2}\frac{9}{2}}\,\mu_B = 7.94\,\mu_B \text{ and } \frac{\lambda_{\text{Eu}^{3+}}}{k_B} = 531.5 \text{ K}$$

	$n_{\text{Eu}^{2+}}$	$\mu_{\text{eff}}(\mu_B)$	θ_{CW} (K)	χ_0 (emu/mol)
EuTaO$_{2.37}$N$_{0.63}$	1	7.44	4.7	2.5×10^{-3}
Eu$_3$Ta$_3$O$_{3.66}$N$_{5.34}$	0.49	7.94 (fixed)	2.4	1.7×10^{-3}

ferromagnetic order should be expected at around this temperature. Indeed, the magnetization data recorded under 25 Oe after zero-field and field-cooling processes (ZFC and FC), shown in Figure 9b, clearly display a hysteretic behavior, developing around 7.5 K. The corresponding field-dependent magnetization loops measured at various temperatures are shown in Figure 9c. The shape of the $M(H)$ curves is consistent with a ferromagnetic ordering, with a saturation

magnetization of about 6 μ_B, closely approaching the nominal 7 μ_B contribution from Eu^{2+} expected for Eu^{2+}Ta$_{0.63}^{5+}$Ta$_{0.37}^{4+}$O$_{2.37}$N$_{0.63}$, and coinciding with the effective moment extracted from susceptibility curves in Figure 9a. Detailed inspection of the low field range in the $M(H)$ data taken at 2 K (Figure 9c (inset)) shows the presence of a minor hysteresis, again consistent with the ferromagnetic character of the sample.

The magnetic data of the nitrogen-richer Eu$_3$Ta$_3$O$_{3.66}$N$_{5.34}$ sample reveals that the effective magnetic moment per Eu ion is largely suppressed and the Curie–Weiss temperature drops by about 50% down to ≈2.4 K. These observations are consistent with the larger fraction of the nonmagnetic Eu^{3+} ions as inferred from $n_{\text{Eu}^{3+}} \approx 0.51$ (Table 2). The corresponding ZFC-FC data (Figure 9b) confirm that ferromagnetic order develops only at lower temperatures (≈3 K). The $M(H)$ curves (Figure 9d) consistently reflect a dramatic reduction of the saturation magnetization (≈3.5 μ_B).

The relative fraction of Eu^{2+} ions in the phase II sample deduced from susceptibility data in Figure 9a ($n_{Eu^{2+}} \approx 0.49$) is larger than expected from chemical analysis ($n_{Eu^{2+}} \approx 0.22$). This difference could originate from the possible existence of anion vacancies, which have not been considered and would increase the proportion of Eu^{2+}, as well as from the extreme simplification of eq 4. For instance, a concentration of oxygen vacancies of 4.7% (0.42 atoms) would lead to $n_{Eu^{2+}} = 0.5$, involving an increase of the fraction of this cation in both A1 and A2 sites of the triple perovskite structure.

All in all, the magnetization data in Figure 9 allow us to conclude that by increasing the N/O ratio in europium tantalum perovskite oxynitrides, the magnetization reduces and the ferromagnetic ordering temperature lowers by the increasing contribution of the nonmagnetic Eu^{3+} in the structure, that dilutes magnetic interaction among Eu^{2+} ions.

CONCLUSIONS

A new high-temperature solid-state synthesis approach under N_2 or N_2/H_2 gas at 1200 °C is used to obtain europium perovskite tantalum oxynitrides with a large range of nitrogen contents, starting with mixtures of Eu_2O_3 and TaON or Eu_2O_3, EuN, and Ta_3N_5. $EuTaO_{2.37}N_{0.63}$ prepared from Eu_2O_3 and TaON under N_2/H_2 shows a simple cubic $Pm\overline{3}m$ perovskite structure whereas the new, highly nitrided compound $Eu_3Ta_3O_{3.66}N_{5.34}$ is prepared from Eu_2O_3, EuN, and Ta_3N_5. $Eu_3Ta_3O_{3.66}N_{5.34}$ with formal stoichiometry $Eu_{2.34}^{3+}Eu_{0.66}^{2+}Ta_3O_{3.66}N_{5.34}$ is a mixed-valence Eu^{2+}/Eu^{3+} compound with long-range order of europium ions in two A sites with different average charge and ratio 2:1, occupied preferentially by Eu^{3+} and Eu^{2+} respectively, that generate well-differentiated coordination environments. This order leads to a triple perovskite structure crystallizing in the $P4/mmm$ space group with parameters $a = a_0$, $c = 3a_0$, where a_0 is the parameter of the cubic perovskite subcell. The new perovskite is ferromagnetic with $T_c \approx 3$ K and saturation magnetization of ≈ 3 μ_B, which are lower than for $EuTaO_{2.37}N_{0.63}$ ($T_c \approx 8$ K, $M_s \approx 6$ μ_B) because of the presence of Eu^{3+}, which has a nonmagnetic ground state and dilutes the magnetic interactions between the Eu^{2+} cations. These findings increase the diversity of crystal structures in the field of perovskite oxynitrides and demonstrate that the synthesis from mixtures of binary nitrides and oxides is very effective in tuning their nitriding degree when cations in different oxidation states can be present by controlling the N/O ratio in the reactants. The same synthetic approach could be extended to other perovskite oxynitrides, potentially leading to new structures and physical properties by expanding the accessed anion compositions of the compounds prepared by ammonolysis.

AUTHOR INFORMATION

Corresponding Authors

Josep Fontcuberta − *Institut de Ciència de Materials de Barcelona (ICMAB-CSIC), 08193 Bellaterra, Spain*; Email: fontcuberta@icmab.cat

Amparo Fuertes − *Institut de Ciència de Materials de Barcelona (ICMAB-CSIC), 08193 Bellaterra, Spain*; ⊙ orcid.org/0000-0001-5338-9724; Email: amparo.fuertes@icmab.es

Authors

Jhonatan R. Guarín − *Institut de Ciència de Materials de Barcelona (ICMAB-CSIC), 08193 Bellaterra, Spain*

Carlos Frontera − *Institut de Ciència de Materials de Barcelona (ICMAB-CSIC), 08193 Bellaterra, Spain*; ⊙ orcid.org/0000-0002-0091-4756

Judith Oró-Solé − *Institut de Ciència de Materials de Barcelona (ICMAB-CSIC), 08193 Bellaterra, Spain*

Jaume Gàzquez − *Institut de Ciència de Materials de Barcelona (ICMAB-CSIC), 08193 Bellaterra, Spain*; ⊙ orcid.org/0000-0002-2561-328X

Clemens Ritter − *Institut Laue-Langevin, Grenoble 38000, France*

Complete contact information is available at: https://pubs.acs.org/10.1021/acs.inorgchem.3c02691

Author Contributions

The manuscript was written with the contributions of all authors. All authors have given approval to the final version of the manuscript.

Notes

The authors declare no competing financial interest.

ACKNOWLEDGMENTS

REFERENCES

(1) Fuertes, A. Nitride Tuning of Transition Metal Perovskites. *APL Mater.* **2020**, *8*, No. 020903.

(2) Yang, M.; Oró-Solé, J.; Rodgers, J. A.; Jorge, A. B.; Fuertes, A.; Attfield, J. P. Anion Order in Perovskite Oxynitrides. *Nat. Chem.* **2011**, *3*, 47−52.

(3) Porter, S. H.; Huang, Z.; Woodward, P. M. Study of Anion Order/Disorder in $RTaN_2O$ (R = La, Ce, Pr) Perovskite Nitride Oxides. *Cryst. Growth Des.* **2014**, *14*, 117−125.

(4) Attfield, J. P. Principles and Applications of Anion Order in Solid Oxynitrides. *Cryst. Growth Des.* **2013**, *13*, 4623−4629.

(5) Ceravola, R.; Oró-Solé, J.; Black, A. P.; Ritter, C.; Puente Orench, I.; Mata, I.; Molins, E.; Frontera, C.; Fuertes, A. Topochemical Synthesis of Cation Ordered Double Perovskite Oxynitrides. *Dalton Trans.* **2017**, *46*, 5128−52131.

(6) Ceravola, R.; Frontera, C.; Oró-Solé, J.; Black, A. P.; Ritter, C.; Mata, I.; Molins, E.; Fontcuberta, J.; Fuertes, A. Topochemical Nitridation of Sr_2FeMoO_6. *Chem. Commun.* **2019**, *55*, 3105−3108.

(7) Ishida, K.; Tassel, C.; Watabe, D.; Takatsu, H.; Brown, C. M.; Nilsen, G. J.; Kageyama, H. Spin Frustration in Double Perovskite Oxides and Oxynitrides: Enhanced Frustration in La_2MnTaO_5N with

a Large Octahedral Rotation. *Inorg. Chem.* **2021**, *60* (2021), 8252−8258.

(8) Ruddlesden, S. N.; Popper, P. New Compounds of the K_2NiF_4 type. *Acta Crystallogr.* **1957**, *10*, 538−539.

(9) Ruddlesden, S. N.; Popper, P. The Compound $Sr_3Ti_2O_7$ and its Structure. *Acta Crystallogr.* **1958**, *11*, 54−55.

(10) Tobías, G.; Oró-Solé, J.; Beltrán-Porter, D.; Fuertes, A. New Family of Ruddlesden-Popper Strontium Niobium Oxynitrides: $(SrO)(SrNbO_{2-x}N)_n$ (n = 1, 2). *Inorg. Chem.* **2001**, *40*, 6867−6869.

(11) Pors, F.; Marchand, R.; Laurent, Y. Nouveaux Oxynitrures A_2TaO_3N (A = Alcalinoterreux) de type structural K_2NiF_4. *Ann. Chim.* **1991**, *16*, 547−551.

(12) Clarke, S. J.; Hardstone, K. A.; Michie, C. W.; Rosseinsky, M. J. High-Temperature Synthesis and Structures of Perovskite and n = 1 Ruddlesden−Popper Tantalum Oxynitrides. *Chem. Mater.* **2002**, *14*, 2664−2669.

(13) Cordes, N.; Nentwig, M.; Eisenburger, L.; Oeckler, O.; Schnick, W. Ammonothermal Synthesis of the Mixed-Valence Nitrogen-Rich Europium Tantalum Ruddlesden-Popper Phase $Eu^{II}Eu_2^{III}Ta_2N_4O_3$. *Eur. J. Inorg. Chem.* **2019**, *2019*, 2304−2311.

(14) Marchand, R. Oxynitrures à Structure K_2NiF_4. Les composés Ln_2AlO_3N (Ln= La, Nd, Sm). *C.R. Acad. Sci.* **1976**, *282*, 329−331.

(15) Dion, M.; Ganne, M.; Tournoux, M. Nouvelle Famille du phases $M^IM_2^{I\ II}Nb_3O_{10}$. *Mater. Res. Bull.* **1981**, *16*, 1429−1435.

(16) Jacobson, A. J.; Johnson, J. W.; Lewandowski, J. T. Interlayer Chemistry between Thick Transition-Metal Oxide Layers: Synthesis and Intercalation Reactions of $K[Ca_2Na_{n-3}Nb_nO_{3n+1}]$ (3 ≤ n ≤ 7). *Inorg. Chem.* **1985**, *24*, 3727−3729.

(17) Schottenfeld, J. A.; Benesi, A. J.; Stephens, P. W.; Chen, G.; Eklund, P. C.; Mallouk, T. E. Structural Analysis and Characterization of Layer Perovskite Oxynitrides made from Dion−Jacobson Oxide Precursors. *J. Solid State Chem.* **2005**, *178*, 2313−2321.

(18) Oshima, T.; Ichibha, T.; Oqmhula, K.; Hibino, K.; Mogi, H.; Yamashita, S.; Fujii, K.; Miseki, Y.; Hongo, K.; Lu, D.; Maezono, R.; Sayama, K.; Yashima, M.; Kimoto, K.; Kato, H.; Kakihana, M.; Kageyama, H.; Maeda, K. Two-Dimensional Perovskite Oxynitride $K_2LaTa_2O_6N$ with an H^+/K^+ Exchangeability in Aqueous Solution Forming a Stable Photocatalyst for Visible-Light H_2 Evolution. *Angew. Chem., Int. Ed.* **2020**, *59*, 9736−9743.

(19) Oró-Solé, J.; Fina, I.; Frontera, C.; Gàzquez, J.; Ritter, C.; Cunquero, M.; Loza-Alvarez, P.; Conejeros, S.; Alemany, P.; Canadell, E.; Fontcuberta, J.; Fuertes, A. Engineering Polar Oxynitrides: Hexagonal Perovskite $BaWON_2$. *Angew. Chem., Int. Ed.* **2020**, *59*, 18395−18399.

(20) Jorge, A. B.; Oró-Solé, J.; Bea, A. M.; Mufti, N.; M Palstra, T. T.; Rodgers, J. A.; Attfield, J. P.; Fuertes, A. Large Coupled Magnetoresponses in $EuNbO_2N$. *J. Am. Chem. Soc.* **2008**, *130*, 12572−12573.

(21) Yang, M.; Oró-Solé, J.; Kusmartseva, A.; Fuertes, A.; Attfield, J. P. Electronic Tuning of Two Metals and Colossal Magnetoresistances in $EuWO_{1+x}N_{2-x}$ Perovskites. *J. Am. Chem. Soc.* **2010**, *132*, 4822−4829.

(22) Mikita, R.; Aharen, T.; Yamamoto, T.; Takeiri, F.; Ya, T.; Yoshimune, W.; Fujita, K.; Yoshida, S.; Tanaka, K.; Batuk, D.; Abakumov, A. M.; Brown, C. M.; Kobayashi, Y.; Kageyama, H. Topochemical Nitridation with Anion Vacancy-Assisted N^{3-}/O^{2-} Exchange. *J. Am. Chem. Soc.* **2016**, *138*, 3211−3217.

(23) Marchand, R.; Pors, F.; Laurent, Y. Nouvelles Perovskites Oxynitrures de Stoechiometrie ABO_2N (A= Lanthanide, B = Ti) et $ABON_2$ (A= Lanthanide, B = Ta ou Nb). *Ann. Chim.* **1991**, *16*, 553−560.

(24) Oró-Solé, J.; Frontera, C.; Black, A. P.; Castets, A.; Velásquez-Méndez, K. L.; Fontcuberta, J.; Fuertes, A. Structural, Magnetic and Electronic Properties of $EuTi_{0.5}W_{0.5}O_{3-x}N_x$ Perovskite Oxynitrides. *J. Solid State Chem.* **2020**, *286*, No. 121274.

(25) Brauer, G.; Weidlein, J.; Strähle, J. Uber das Tantalnitrid Ta_3N_5 und das Tantaloxidnitrid TaON. *Z. Anorg. Allg. Chem.* **1966**, *348*, 298−308.

(26) Fauth, F.; Peral, I.; Popescu, C.; Knapp, M. The New Material Science Powder Diffraction Beamline at ALBA Synchrotron. *Powder Diffr.* **2013**, *28*, S360−S370.

(27) Rodríguez-Carvajal, J. Recent Advances in Magnetic Structure Determination by Neutron Powder Diffraction. *Phys. B* **1993**, *192*, 55−69.

(28) Castets, A.; Fina, I.; Guarín, J. R.; Oró-Solé, J.; Frontera, C.; Ritter, C.; Fontcuberta, J.; Fuertes, A. High-Temperature Synthesis and Dielectric Properties of $LaTaON_2$. *Inorg. Chem.* **2021**, *60*, 16484−16491.

(29) Sakata, T.; Yoshiyuki, R.; Okada, R.; Urushidani, S.; Tarutani, N.; Katagiri, K.; Inumaru, K.; Koyama, K.; Masubuchi, Y. Environmentally Benign Synthesis and Color Tuning of Strontium−Tantalum Perovskite Oxynitride and its Solid Solutions. *Inorg. Chem.* **2021**, *60*, 4852−4859.

(30) Bubeck, C.; Widenmeyer, M.; Richter, G.; Coduri, M.; Goering, E.; Yoon, S.; Weidenkaff, A. Tailoring of an Unusual Oxidation State in a Lanthanum Tantalum(IV) Oxynitride Via Precursor Microstructure Design. *Comm. Chem.* **2019**, *2*, 134.

(31) Shannon, R. D. Revised Effective Ionic Radii and Systematic Studies of Interatomic Distances in Halides and Chalcogenides. *Acta Crystallogr., Sect. A: Cryst. Phys., Diffr., Theor. Gen. Crystallogr.* **1976**, *32*, 751−767.

(32) Serrate, D.; De Teresa, J. M.; Ibarra, M. R. Double Perovskites with Ferromagnetism above Room Temperature. *J. Phys.: Condens. Matter* **2007**, *9*, No. 023201.

(33) Andruh, M.; Bakalbassis, E.; Kahn, O.; Trombe, J. C.; Porcher, P. Structure, Spectroscopic and Magnetic Properties of Rare Earth Metal(III) Derivatives with the 2-formyl-4-methyl-6-(N-(2-pyridylethyl)formimidoyl)phenol Ligand. *Inorg. Chem.* **1993**, *32*, 1616−1622.

(34) Zong, Y.; Fujita, K.; Akamatsu, H.; Murai, S.; Tanaka, K. Antiferromagnetism of Perovskite $EuZrO_3$. *J. Solid State Chem.* **2010**, *183*, 168−172.